A lattice Boltzmann model for reactive mixtures

Author(s):
Sawant, Nilesh; Dorschner, Benedikt; Karlin, Iliya V.

Publication date:
2021-10-18

Permanent link:
https://doi.org/10.3929/ethz-b-000505641

Originally published in:
Philosophical Transactions of the Royal Society A: Mathematical, Physical and Engineering Sciences 379(2208), https://doi.org/10.1098/rsta.2020.0402

Funding acknowledgement:
834763 - Particles-on-Demand for Multiscale Fluid Dynamics (EC)

PHILOSOPHICAL TRANSACTIONS A

royalsocietypublishing.org/journal/rsta

Research

Cite this article: Sawant N, Dorschner B, Karlin IV. 2021 A lattice Boltzmann model for reactive mixtures. *Phil. Trans. R. Soc. A* **379**: 20200402.
https://doi.org/10.1098/rsta.2020.0402

Accepted: 21 February 2021

One contribution of 15 to a theme issue 'Progress in mesoscale methods for fluid dynamics simulation'.

Subject Areas:
fluid mechanics, statistical physics, mechanical engineering, computer modelling and simulation, computational physics, reactive flows, combustion

Keywords:
reactive lattice Boltzmann, Stefan-Maxwell diffusion, multicomponent lattice Boltzmann, circular expanding flame, detailed chemistry lattice Boltzmann, lattice Boltzmann hydrogen air

Author for correspondence:
I. V. Karlin
e-mail: ikarlin@ethz.ch

A lattice Boltzmann model for reactive mixtures

N. Sawant, B. Dorschner and I. V. Karlin

Department of Mechanical and Process Engineering, ETH Zurich, 8092 Zurich, Switzerland

NS, 0000-0001-8403-8943; IVK, 0000-0001-9996-9679

A new lattice Boltzmann model for reactive ideal gas mixtures is presented. The model is an extension to reactive flows of the recently proposed multi-component lattice Boltzmann model for compressible ideal gas mixtures with Stefan–Maxwell diffusion for species interaction. First, the kinetic model for the Stefan–Maxwell diffusion is enhanced to accommodate a source term accounting for the change in the mixture composition due to chemical reaction. Second, by including the heat of formation in the energy equation, the thermodynamic consistency of the underlying compressible lattice Boltzmann model for momentum and energy allows a realization of the energy and temperature change due to chemical reactions. This obviates the need for ad-hoc modelling with source terms for temperature or heat. Both parts remain consistently coupled through mixture composition, momentum, pressure, energy and enthalpy. The proposed model uses the standard three-dimensional lattices and is validated with a set of benchmarks including laminar burning speed in the hydrogen–air mixture and circular expanding premixed flame.

This article is part of the theme issue 'Progress in mesoscale methods for fluid dynamics simulation'.

1. Introduction

The lattice Boltzmann method (LBM) is a recast of fluid dynamics into a fully discrete kinetic system for the populations $f_i(\boldsymbol{x}, t)$ of designer particles, which are associated with the discrete velocities $\boldsymbol{c}_i$ fitting into a regular space-filling lattice. As a result, the kinetic equations for the populations $f_i(\boldsymbol{x}, t)$ follow a simple

THE ROYAL SOCIETY PUBLISHING

algorithm of 'stream along links $\boldsymbol{c}_i$ and collide at the nodes $\boldsymbol{x}$ in discrete time t'. LBM has been successfully applied to a range of problems in fluid dynamics including but not limited to transitional flows, flows in complex moving geometries compressible flows, multiphase flows and rarefied gas, to name a few [1,2].

Nevertheless, in spite of extensive development, the multicomponent reactive mixtures so far resisted a significant advancement in the LBM context. Arguably, one of the main reasons was the absence of a thermodynamically consistent LBM for mixtures. Early approaches such as [3,4] suffer many limitations such as incompressible flow restriction, constant transport properties and rudimentary diffusion modelling.

As a remedy, a number of recent works [5–10] abandoned the construction of a kinetic model or LBM for multicomponent mixtures in favour of a so-called hybrid LBM where only the flow of the mixture is represented by an (augmented) LBM equation while the species and the temperature dynamics are modelled by conventional macroscopic equations. While the hybrid LBM approach can be potentially useful, in particular for combustion applications, our goal here is to retain a fully kinetic model and LBM for multicomponent reactive mixtures.

Recently, we proposed a novel lattice Boltzmann framework for compressible multicomponent mixtures with a realistic equation of state and thermodynamic consistency [11]. The strongly coupled formulation consists of kinetic equations for momentum, energy and species dynamics and was validated for a variety of test cases involving uphill diffusion, opposed jets and Kelvin–Helmholtz instability. This extends the LBM to realistic mixtures and opens the door for reactive flow applications with a fully kinetic approach, which is the subject of this paper. We propose a fully kinetic, strongly coupled lattice Boltzmann model for compressible reactive flows as an extension of [11]. To that end, a generic M-component ideal gas mixture is represented by two sets of kinetic equations. A set of M kinetic equations is used to model species undergoing Stefan–Maxwell diffusion. This set is now extended to include the reaction source term. Furthermore, the mixture is described by a set of two kinetic equations, where one accounts for the total mass and momentum of the mixture and another for the total energy of the mixture. The kinetic equation for the mixture energy is extended to also include the internal energy of formation in addition to the sensible internal energy. Thus, the approach presented here can accurately model a reactive M-component compressible mixture with $M+2$ kinetic equations. The system is fully coupled through mixture composition, momentum, pressure and enthalpy. The thermodynamic consistency of the model allows us to automatically account for the energy changes due to chemical reactions. The Stefan–Maxwell diffusion is retained and thus complicated phenomena such as reverse diffusion, osmotic diffusion or diffusion barrier can be captured, as was already demonstrated in the non-reactive case in [11].

The outline of the paper is as follows. In §2, we extend the lattice Boltzmann model of [11] to the reactive multicomponent mixtures. This is achieved by supplying a reaction source term to the kinetic equations for the species in such a way that the Stefan–Maxwell diffusion mechanism already implemented by the model stays intact. In §3, we extend the two-population lattice Boltzmann model for the mixture flow and energy to include the enthalpy of formation of chemically reacting species. Thanks to the thermodynamic consistency featured by the original model [11], this final step completes the construction of the lattice Boltzmann model for the reactive mixtures. The derivation follows the path presented in detail in [11], and we indicate the differences brought about by the thermodynamics of the chemical reaction. In §4, we outline the coupling of the lattice Boltzmann solver with the open source chemical kinetics package Cantera. Validation of the model is presented in §5 with the simulation of detailed hydrogen/air combustion mechanism and the discussion is provided in §6.

2. Lattice Boltzmann model for the species

The composition of a reactive mixture of M ideal gases is described by the species densities ρ_a, $a=1,\ldots,M$, while the mixture density is $\rho=\sum_{a=1}^{M}\rho_a$. The rate of change of ρ_a due to chemical

reaction $\dot{\rho}_a^c$ satisfies mass conservation,

$$\sum_{a=1}^{M} \dot{\rho}_a^c = 0. \tag{2.1}$$

Introducing the mass fraction $Y_a = \rho_a/\rho$, the molar mass of the mixture m is given by $m^{-1} = \sum_{a=1}^{M} Y_a/m_a$, where m_a is the molar mass of the component a. The equation of state of the mixture provides a relation between the pressure P, the temperature T and the composition,

$$P = \rho RT, \tag{2.2}$$

where $R = R_U/m$ is the specific gas constant of the mixture and R_U is the universal gas constant. The pressure of an individual component P_a is related to the pressure of the mixture P through Dalton's Law of partial pressures, $P_a = X_a P$, where the mole fraction of a component X_a is related to its mass fraction Y_a as $X_a = mY_a/m_a$. Combined with the equation of state (2.2), the partial pressure P_a takes the form $P_a = \rho_a R_a T$, where $R_a = R_U/m_a$ is the specific gas constant of the component. A kinetic model for the Stefan–Maxwell diffusion in the non-reactive mixture was introduced in [11]. Here, we extend the formulation [11] to include the reaction. To that end, we write the kinetic equation for the populations f_{ai}, $a = 1, \ldots, M$, of the component a, corresponding to the discrete velocities $\boldsymbol{c}_i$, $i = 0, \ldots, Q-1$,

$$\partial_t f_{ai} + \boldsymbol{c}_i \cdot \nabla f_{ai} = \sum_{b \neq a}^{M} \frac{P X_a X_b}{\mathcal{D}_{ab}} \left[\left(\frac{f_{ai}^{\mathrm{eq}} - f_{ai}}{\rho_a} \right) - \left(\frac{f_{bi}^{\mathrm{eq}} - f_{bi}^{*}}{\rho_b} \right) \right] + \dot{f}_{ai}^{c}. \tag{2.3}$$

Here $\mathcal{D}_{ab}$ are the binary diffusivity coefficients. The species' densities ρ_a and partial momenta $\rho_a \boldsymbol{u}_a$ are, respectively,

$$\rho_a = \sum_{i=0}^{Q-1} f_{ai} \quad \text{and} \quad \rho_a \boldsymbol{u}_a = \sum_{i=0}^{Q-1} f_{ai} \boldsymbol{c}_i. \tag{2.4}$$

The momenta of the components sum up to the mixture momentum, At variance with the non-reactive mixture [11], kinetic equation (2.3) includes a source term $\dot{f}_{ai}^c$ which implements the rate of change of ρ_a due to the reaction and satisfies the following conditions,

$$\sum_{i=0}^{Q-1} \dot{f}_{ai}^c = \dot{\rho}_a^c \quad \text{and} \quad \sum_{i=0}^{Q-1} \dot{f}_{ai}^c \boldsymbol{c}_i = \dot{\rho}_a^c \boldsymbol{u}. \tag{2.5}$$

The kinetic model (2.3) is realized on the standard three-dimensional $D3Q27$ lattice with the discrete velocities $\boldsymbol{c}_i = (c_{ix}, c_{iy}, c_{iz})$, $c_{i\alpha} \in \{-1, 0, 1\}$. As in [11], the equilibrium f_{ai}^{eq} and the quasi-equilibrium f_{ai}^{*} in (2.3) are constructed using the product-form [12]: we define a triplet of functions in two variables, ξ and $\zeta > 0$,

$$\Psi_0(\xi, \zeta) = 1 - (\xi^2 + \zeta), \quad \Psi_1(\xi, \zeta) = \frac{\xi + (\xi^2 + \zeta)}{2} \quad \text{and} \quad \Psi_{-1}(\xi, \zeta) = \frac{-\xi + (\xi^2 + \zeta)}{2}. \tag{2.6}$$

The equilibrium f_{ai}^{eq} and the quasi-equilibrium f_{ai}^{*} populations are evaluated as the products of the functions (2.6), with $\xi = u_\alpha$ and $\xi = u_{a\alpha}$, respectively, and with $\zeta = R_a T$ in both cases,

$$f_{ai}^{\mathrm{eq}}(\rho_a, \boldsymbol{u}, R_a T) = \rho_a \Psi_{c_{ix}}(u_x, R_a T)\, \Psi_{c_{iy}}(u_y, R_a T)\, \Psi_{c_{iz}}(u_z, R_a T) \tag{2.7}$$

and

$$f_{ai}^{*}(\rho_a, \boldsymbol{u_a}, R_a T) = \rho_a \Psi_{c_{ix}}(u_{ax}, R_a T)\, \Psi_{c_{iy}}(u_{ay}, R_a T)\, \Psi_{c_{iz}}(u_{az}, R_a T)\,. \tag{2.8}$$

The reaction source term $\dot{f}_{ai}^c$ in (2.3) is also represented by the product-form similar to (2.7),

$$\dot{f}_{ai}^{c}(\dot{\rho}_a^c, \boldsymbol{u}, R_a T) = \dot{\rho}_a^c \Psi_{c_{ix}}(u_x, R_a T)\, \Psi_{c_{iy}}(u_y, R_a T)\, \Psi_{c_{iz}}(u_z, R_a T)\,. \tag{2.9}$$

The analysis of the hydrodynamic limit of the kinetic model (2.3) follows the lines already presented in [11]. Note that the constraint on the momentum of the source term (2.5) is required.

The balance equations for the densities of the species in the presence of the source term are found as follows:

$$\partial_t \rho_a = -\nabla \cdot (\rho_a \boldsymbol{u}) - \nabla \cdot (\rho_a \delta \boldsymbol{u}_a) + \dot{\rho}_a^c, \tag{2.10}$$

where the diffusion velocities, $\delta \boldsymbol{u}_a = \boldsymbol{u}_a - \boldsymbol{u}$, satisfy the Stefan–Maxwell constitutive relation,

$$P \nabla X_a + (X_a - Y_a) \nabla P = \sum_{b \neq a}^{M} \frac{P X_a X_b}{\mathcal{D}_{ab}} (\delta \boldsymbol{u}_b - \delta \boldsymbol{u}_a). \tag{2.11}$$

Summarizing, kinetic model (2.3) recovers both the Stefan–Maxwell law of diffusion and the contribution of the species mass change due to chemical reaction, as presented in equation (2.10).

Derivation of the lattice Boltzmann equation from the kinetic model (2.3) proceeds along the lines of the non-reactive case [11]. Upon integration of (2.3) along the characteristics and application of the trapezoidal rule, we arrive at a fully discrete lattice Boltzmann equation

$$f_{ai}(\boldsymbol{x} + \boldsymbol{c}_i \delta t, t + \delta t) = f_{ai}(\boldsymbol{x}, t) + 2\beta_a [f_{ai}^{\mathrm{eq}}(\boldsymbol{x}, t) - f_{ai}(\boldsymbol{x}, t)] + \delta t (\beta_a - 1) F_{ai}(\boldsymbol{x}, t) + \delta t \dot{f}_{ai}^c. \tag{2.12}$$

The discrete equation (2.12) is used in the actual numerical implementation. Unlike equation (2.3), the discrete equation does not contain species mass in the denominator. Therefore, no special treatment is required for species masses going to zero. The short-hand notation F_{ai} for the inter-species interaction term and the relaxation parameters $\beta_a \in [0, 1]$ are,

$$F_{ai} = Y_a \sum_{b \neq a}^{M} \frac{1}{\tau_{ab}} \left(f_{bi}^{\mathrm{eq}} - f_{bi}^{*} \right), \quad \beta_a = \frac{\delta t}{2\tau_a + \delta t}, \tag{2.13}$$

where the characteristic times τ_{ab} and the relaxation times τ_a are related to the binary diffusivities,

$$\tau_{ab} = \left(\frac{m_a m_b}{m R_U T} \right) \mathcal{D}_{ab}, \quad \frac{1}{\tau_a} = \sum_{b \neq a}^{M} \frac{Y_b}{\tau_{ab}}. \tag{2.14}$$

Furthermore, the quasi-equilibrium populations $f_{bi}^{*} = f_{bi}^{*}(\rho_b, \boldsymbol{u} + \delta \boldsymbol{u}_b, R_b T)$ in the expression F_{ai} (2.13) depend on the diffusion velocity $\delta \boldsymbol{u}_b$. The latter are found by solving the $M \times M$ linear algebraic system for each spatial component

$$\left(1 + \frac{\delta t}{2\tau_a} \right) \delta \boldsymbol{u}_a - \frac{\delta t}{2} \sum_{b \neq a}^{M} \frac{1}{\tau_{ab}} Y_b \delta \boldsymbol{u}_b = \boldsymbol{u}_a - \boldsymbol{u}. \tag{2.15}$$

The linear algebraic system was already derived in [11] for the non-reactive mixtures and is not altered by the presence of the reaction source term. The equilibrium population $f_{ai}^{\mathrm{eq}} = f_{ai}^{\mathrm{eq}}(\rho_a, \boldsymbol{u}, R_a T)$ and the reaction source term $\dot{f}_{ai}^c = \dot{f}_{ai}^c(\dot{\rho}_a, \boldsymbol{u}, R_a T)$ in (2.12) and (2.13) are evaluated at the mixture velocity $\boldsymbol{u}$. Summarizing, the lattice Boltzmann system (2.12) delivers the extension of the species dynamics subject to the Stefan–Maxwell diffusion to the reactive mixtures. We proceed with the extension of the flow and energy dynamics of the mixture.

3. Lattice Boltzmann model of mixture momentum and energy

The mass-based specific internal energy U_a and enthalpy H_a of a species a are,

$$U_a = U_a^0 + \int_{T_0}^{T} C_{a,v}(T') \, \mathrm{d}T' \quad \text{and} \quad H_a = H_a^0 + \int_{T_0}^{T} C_{a,p}(T') \, \mathrm{d}T', \tag{3.1}$$

where U_a^0 and H_a^0 are, respectively, the energy and the enthalpy of formation at the reference temperature T_0, while $C_{a,v}$ and $C_{a,p}$ are specific heats at constant volume and at constant pressure, respectively. The internal energy ρU and the enthalpy ρH of a mixture are

$$\rho U = \sum_{a=1}^{M} \rho_a U_a \quad \text{and} \quad \rho H = \sum_{a=1}^{M} \rho_a H_a. \tag{3.2}$$

While the sensible heat was considered in the non-reactive case [11], by taking into account the heat of formation we immediately extend the model to reactive mixtures. As in [11], we follow a two-population approach. One set of populations (f-populations) is used to represent the density and the momentum of the mixture

$$\sum_{i=0}^{Q-1} f_i = \rho \quad \text{and} \quad \sum_{i=0}^{Q-1} f_i \boldsymbol{c}_i = \rho \boldsymbol{u}. \tag{3.3}$$

Another set (g-populations) represents the total energy,

$$\sum_{i=0}^{Q-1} g_i = \rho E, \quad \rho E = \rho U + \frac{\rho u^2}{2}. \tag{3.4}$$

A coupling between the mixture and the species kinetic equations is established through energy since the mixture internal energy (3.2) depends on the composition. Furthermore, the temperature is evaluated by solving the integral equation, cf. (3.1) and (3.2),

$$\sum_{a=1}^{M} Y_a \left[U_a^0 + \int_{T_0}^{T} C_{a,v}(T')\, \mathrm{d}T' \right] = E - \frac{u^2}{2}. \tag{3.5}$$

The temperature is used as the input for the equation of state (2.2) and hence in the equilibrium, the quasi-equilibrium and the reaction source term of the species lattice Boltzmann system which leads to a two-way coupling between the species and the mixture kinetic systems. As in [11], the lattice Boltzmann equations for the f- and g-populations are realized on the $D3Q27$ discrete velocity set

$$f_i(\boldsymbol{x} + \boldsymbol{c}_i \delta t, t + \delta t) - f_i(\boldsymbol{x}, t) = \omega(f_i^{\mathrm{eq}} - f_i) + \boldsymbol{A}_i \cdot \boldsymbol{X} \tag{3.6}$$

and

$$g_i(\boldsymbol{x} + \boldsymbol{c}_i \delta t, t + \delta t) - g_i(\boldsymbol{x}, t) = \omega_1(g_i^{\mathrm{eq}} - g_i) + (\omega - \omega_1)(g_i^{*} - g_i), \tag{3.7}$$

where relaxation parameters ω and ω_1 are related to the viscosity and thermal conductivity. The equilibrium f-populations f_i^{eq} in (3.6) are evaluated using the product-form, with $\xi_\alpha = u_\alpha$ and $\zeta = RT$ in (2.6),

$$f_i^{\mathrm{eq}}(\rho, \boldsymbol{u}, RT) = \rho \Psi_{c_{ix}}(u_x, RT)\, \Psi_{c_{iy}}\left(u_y, RT\right) \Psi_{c_{iz}}(u_z, RT)\,. \tag{3.8}$$

The last term in (3.6) is a correction needed to compensate for the insufficient isotropy of the $D3Q27$ lattice in the compressible flow setting [11,13–15]: $\boldsymbol{X}$ is the vector with the components

$$X_\alpha = -\partial_\alpha \left[\left(\frac{1}{\omega} - \frac{1}{2} \right) \delta t \partial_\alpha (\rho u_\alpha (1 - 3RT) - \rho u_\alpha^3) \right], \tag{3.9}$$

while the components of vectors $\boldsymbol{A}_i$ are defined as

$$A_{i\alpha} = \frac{1}{2} c_{i\alpha} \text{ for } c_i^2 = 1; \quad A_{i\alpha} = 0 \text{ otherwise.} \tag{3.10}$$

The equilibrium and the quasi-equilibrium g-populations, g_i^{eq} and g_i^{*} in (3.7), are defined with the help of Grad's approximation [16],

$$g_i^{\mathrm{eq}} = w_i \left(\rho E + \frac{\boldsymbol{q}^{\mathrm{eq}} \cdot \boldsymbol{c}_i}{\theta} + \frac{(\boldsymbol{R}^{\mathrm{eq}} - \rho E \theta \boldsymbol{I}) : (\boldsymbol{c}_i \otimes \boldsymbol{c}_i - \theta \boldsymbol{I})}{2\theta^2} \right) \tag{3.11}$$

and

$$g_i^* = w_i \left(\rho E + \frac{\boldsymbol{q}^* \cdot \boldsymbol{c}_i}{\theta} + \frac{(\boldsymbol{R}^{\mathrm{eq}} - \rho E \theta \boldsymbol{I}) : (\boldsymbol{c}_i \otimes \boldsymbol{c}_i - \theta \boldsymbol{I})}{2\theta^2} \right). \tag{3.12}$$

Here, the weights $w_i = w_{c_{ix}} w_{c_{iy}} w_{c_{iz}}$ are the products of the one-dimensional weights $w_0 = 1 - \theta$, $w_1 = w_{-1} = \theta/2$, and $\theta = 1/3$ is the lattice reference temperature. The equilibrium mixture energy flux $\boldsymbol{q}^{\mathrm{eq}}$ and the second-order moment tensor $\boldsymbol{R}^{\mathrm{eq}}$ in (3.11) and (3.12) are

$$\boldsymbol{q}^{\mathrm{eq}} = \sum_{i=0}^{Q-1} g_i^{\mathrm{eq}} \boldsymbol{c}_i = \left(H + \frac{u^2}{2} \right) \rho \boldsymbol{u} \tag{3.13}$$

and

$$\boldsymbol{R}^{\mathrm{eq}} = \sum_{i=0}^{Q-1} g_i^{\mathrm{eq}} \boldsymbol{c}_i \otimes \boldsymbol{c}_i = \left(H + \frac{u^2}{2} \right) \boldsymbol{P}^{\mathrm{eq}} + P \boldsymbol{u} \otimes \boldsymbol{u}, \tag{3.14}$$

where H is the specific mixture enthalpy (3.2). The quasi-equilibrium energy flux $\boldsymbol{q}^*$ in (3.12) has the following form:

$$\boldsymbol{q}^* = \sum_{i=0}^{Q-1} g_i^* \boldsymbol{c}_i = \boldsymbol{q} - \boldsymbol{u} \cdot (\boldsymbol{P} - \boldsymbol{P}^{\mathrm{eq}}) + \boldsymbol{q}^{\mathrm{diff}} + \boldsymbol{q}^{\mathrm{corr}}. \tag{3.15}$$

The first two terms in (3.15) include the energy flux $\boldsymbol{q}$ and the pressure tensor $\boldsymbol{P}$,

$$\boldsymbol{q} = \sum_{i=0}^{Q-1} g_i \boldsymbol{c}_i, \quad \boldsymbol{P} = \sum_{i=0}^{Q-1} f_i \boldsymbol{c}_i \otimes \boldsymbol{c}_i. \tag{3.16}$$

Their contribution maintains a variable Prandtl number and is patterned from the single-component case [13]. The remaining two terms in the quasi-equilibrium energy flux (3.15), $\boldsymbol{q}^{\mathrm{diff}}$ and $\boldsymbol{q}^{\mathrm{corr}}$ pertain to the multicomponent case. The interdiffusion energy flux $\boldsymbol{q}^{\mathrm{diff}}$ is

$$\boldsymbol{q}^{\mathrm{diff}} = \left(\frac{\omega_1}{\omega - \omega_1} \right) \rho \sum_{a=1}^{M} H_a Y_a \delta \boldsymbol{u}_a, \tag{3.17}$$

where the diffusion velocities $\delta \boldsymbol{u}_a$ are defined according to equation (2.15). The flux (3.17) contributes the enthalpy transport due to diffusion and hence it vanishes in the single-component case but is significant in reactive flows. Finally, the correction flux $\boldsymbol{q}^{\mathrm{corr}}$, which also vanishes in the single-component case, is required in the two-population approach to the mixtures in order to recover the Fourier law of thermal conduction, see [11] for details,

$$\boldsymbol{q}^{\mathrm{corr}} = \frac{1}{2} \left(\frac{\omega_1 - 2}{\omega_1 - \omega} \right) \delta t P \sum_{a=1}^{M} H_a \nabla Y_a. \tag{3.18}$$

Prefactors featured in (3.17) and (3.18) were found in [11] based on the analysis of the hydrodynamic limit of the lattice Boltzmann system (3.6) and (3.7) and are not affected by the present reactive mixture case. Second-order accurate isotropic lattice operators proposed in [17] were used for the evaluation of spatial derivatives in the correction flux (3.18) as well as in the isotropy correction (3.9). Following [11], the continuity, the momentum and the energy equations for a reactive multicomponent mixture [18] are obtained as follows:

$$\partial_t \rho + \nabla \cdot (\rho \boldsymbol{u}) = 0, \tag{3.19}$$

$$\partial_t (\rho \boldsymbol{u}) + \nabla \cdot (\rho \boldsymbol{u} \otimes \boldsymbol{u}) + \nabla \cdot \boldsymbol{\pi} = 0 \tag{3.20}$$

and

$$\partial_t (\rho E) + \nabla \cdot (\rho E \boldsymbol{u}) + \nabla \cdot \boldsymbol{q} + \nabla \cdot (\boldsymbol{\pi} \cdot \boldsymbol{u}) = 0. \tag{3.21}$$

The pressure tensor $\boldsymbol{\pi}$ in the momentum equation (3.20) reads

$$\boldsymbol{\pi} = P\boldsymbol{I} - \mu\left(\nabla\boldsymbol{u} + \nabla\boldsymbol{u}^{\dagger} - \frac{2}{D}(\nabla\cdot\boldsymbol{u})\boldsymbol{I}\right) - \varsigma(\nabla\cdot\boldsymbol{u})\boldsymbol{I}, \tag{3.22}$$

where the dynamic viscosity μ and the bulk viscosity ς are related to the relaxation parameter ω,

$$\mu = \left(\frac{1}{\omega} - \frac{1}{2}\right)P\delta t \quad \text{and} \quad \varsigma = \left(\frac{1}{\omega} - \frac{1}{2}\right)\left(\frac{2}{D} - \frac{R}{C_v}\right)P\delta t, \tag{3.23}$$

where $C_v = \sum_{a=1}^{M} Y_a C_{a,v}$ is the mixture specific heat at constant volume. The heat flux $\boldsymbol{q}$ in the energy equation (3.21) reads

$$\boldsymbol{q} = -\lambda\nabla T + \rho\sum_{a=1}^{M} H_a Y_a \delta\boldsymbol{u}_a. \tag{3.24}$$

The first term is the Fourier law of thermal conduction, with the thermal conductivity λ related to the relaxation parameter ω_1,

$$\lambda = \left(\frac{1}{\omega_1} - \frac{1}{2}\right)PC_p\delta t, \tag{3.25}$$

where $C_p = C_v + R$ is the mixture specific heat at constant pressure. The second term in (3.24) is the interdiffusion energy flux. The dynamic viscosity μ and the thermal conductivity λ of the mixture are evaluated as a function of the local composition, temperature and pressure using the chemical kinetics solver Cantera [19], wherein a combination of methods involving interaction potential energy functions [20], hard sphere approximations and the methods described in [21,22] are employed to calculate the mixture transport coefficients. Finally, in accordance with a principle of strong coupling [11], the excess conservation laws arising due to a separated construction of the species diffusion model in §2 and the two-population mixture model are eliminated by removing one set of species populations (here, the component M),

$$f_{Mi} = f_i - \sum_{a=1}^{M-1} f_{ai}. \tag{3.26}$$

Thus, the component M is not an independent field any more but is slaved to the remaining $M-1$ species and the mixture f-populations. Summarizing, the thermodynamically consistent framework of [11] allows for a straightforward extension to reactive mixtures provided the sensible energy and enthalpy are extended to include the energy and the enthalpy of formation.

4. Coupling between lattice Boltzmann and chemical kinetics

In this work, the lattice Boltzmann code is coupled to the open source code chemical kinetics solver Cantera [19]. The Cantera solver is supplied with the publicly accessible GRI-Mech 3.0 mechanism [23] as an input data file. The communication between the lattice Boltzmann solver and the Cantera chemical kinetics solver can be summarized as follows:

(i) An input from the lattice Boltzmann solver to Cantera is provided during the collision step in terms of internal energy, specific volume and mass fractions.
(ii) Cantera internally solves numerically the integral equation (3.5) and thus the temperature at that state is obtained.
(iii) Cantera calculates the production rates of species $\dot{\rho}_a^c$ and the transport coefficients including dynamic viscosity, thermal conductivity and the Stefan–Maxwell diffusivities as a function of the current state.
(iv) The temperature obtained from Cantera is used to evaluate the equilibrium and quasi-equilibrium moments and populations. The transport coefficients are used to calculate the corresponding relaxation times and thus the collision step is complete.

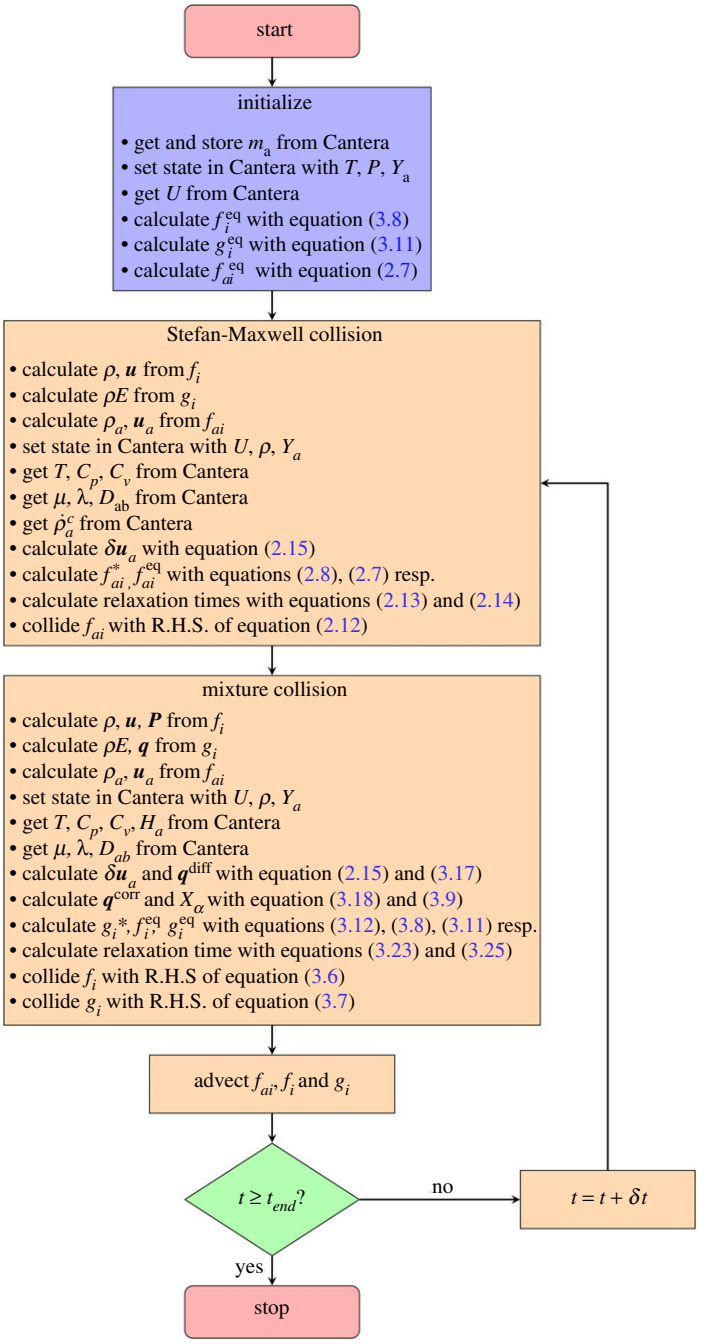

Figure 1. Flowchart for the coupled lattice Boltzmann–Cantera solver. (Online version in colour.)

Other thermodynamic parameters necessary for the simulations such as the specific heats and molecular masses are also obtained through Cantera. The reference standard state temperature is $T_0 = 298.15\,\mathrm{K}$ and the reference standard state pressure is $P_0 = 1\,\mathrm{atm}$. The data required by the lattice Boltzmann solver during runtime is obtained by querying Cantera through its C++ API using the 'IdealGasMix' and 'Transport' classes. A flowchart of the coupling between the lattice Boltzmann solver and the chemical kinetics solver Cantera is sketched in figure 1. The diffusivities

obtained from Cantera are converted to lattice units through the non-dimensional Prandtl number $Pr = \nu/\alpha$ and the Lewis number $Le_{ab} = \alpha/\mathcal{D}_{ab}$. Here, $\alpha = \lambda/(\rho C_p)$ is the thermal diffusivity of the mixture.

5. Results

To test the coupling between the lattice Boltzmann solver and the chemical kinetics solver, we begin by verifying the perfectly stirred reactor set-up with homogeneous hydrogen/air mixture. Next, as a second validation, probing the basic validity of our model, we compute the flame speed in a premixed hydrogen/air mixture with the reactive Stefan–Maxwell formulation in a wide range of equivalence ratios ϕ. Subsequently, in order to test the isotropy of the model, the problem of outward expanding circular flame [24,25] is solved for the premixed hydrogen/air mixture. For both test cases, we use the detailed chemical kinetics mechanism [26] involving the following nine species: N_2, O_2, H_2, H, O, OH, H_2O, HO_2, H_2O_2. It is worthwhile to mention that the model is not restricted to the detailed mechanisms. Reduced mechanisms available in the literature such as the five-species propane mechanism have also been tested with this model. In this paper, we will restrict ourselves to the more interesting detailed hydrogen/air mechanism which forms sharper and faster propagating flames. While this benchmark not only probes the model's behaviour in two dimensions, it is also a stringent isotropy test where it is crucial that the circular shape of the flame is preserved and not contaminated or distorted by the errors of the discrete numerics on the underlying Cartesian grid. Finally, the model's ability to capture nonlinear instabilities is probed by simulations of wrinkled flames, which form as a result of monochromatic perturbations.

(a) Perfectly stirred reactor

To verify the coupling between the lattice Boltzmann solver and the chemical kinetics solver, we simulate a constant volume reactor. The set-up consists of a three-dimensional domain of $4 \times 4 \times 4$ lattice points with periodic boundary conditions in all directions. Stagnant hydrogen/air mixture at an equivalence ratio $\phi = 1$ is initialized with the pressure $P_{\text{in}} = 1\,\text{atm}$ and the temperature $T = 1400\,\text{K}$. The results are compared to the 'IdealGasReactor' class of Cantera using the 'advance' method to march the state of the reactor forward in time. Figure 2*a* shows the history of the temperature and the mass fraction of hydroxide OH. Accurate match with the results obtained from Cantera shows that the coupling has been done correctly. For this problem, since all the boundaries are periodic, the total energy of the system has to remain constant while no kinetic energy should develop over time. Figure 2*b* verifies that in the absence of kinetic energy, the total energy of the solver equals the kinetic energy. Also, the total energy does not deviate from its initial value in this set-up, as expected.

(b) Laminar flame speed

In order to validate our model, we calculate the burning velocity of a hydrogen/air mixture in a one-dimensional set-up. As illustrated in figure 3, the set-up consists of a one-dimensional tube initialized with unburnt mixture at $T_{\text{u}} = 300\,\text{K}$ throughout from the left end up to 80% of the domain towards the right. The remaining 20% of the domain is initialized with the adiabatic flame temperature T_{af} and with the equilibrium burnt composition at the respective equivalence ratio. The pressure is initialized uniformly at $P_{\text{in}} = 1\,\text{atm}$. Zero gradient boundary conditions are used at both ends for all variables using equilibrium populations. At the left end, the velocity is imposed to be zero so that the flame propagates from right to left into the stationary unburnt mixture. The set-up is used to calculate the burning velocity of the premixed $H_2N_2O_2$ system. Nitrogen is considered as an inert gas and thus does not split or form any radicals like nitrous oxides. However, the heat capacity of the inert gas has a strong influence on the flame temperature and consequently on the burning velocity. This is naturally accounted for in the formulation. The

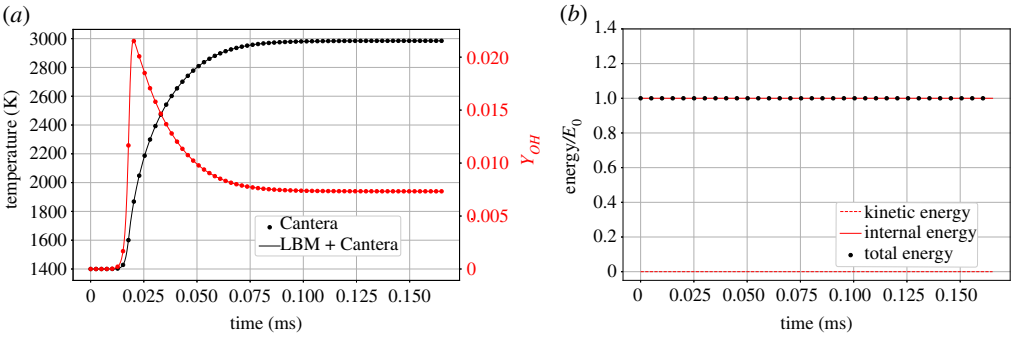

Figure 2. Simulation of hydrogen/air constant volume perfectly stirred reactor. (*a*) Time evolution of temperature and OH mass fraction, (*b*) time evolution of the kinetic, internal and total energy. All quantities are scaled by the initial total energy E_0. (Online version in colour.)

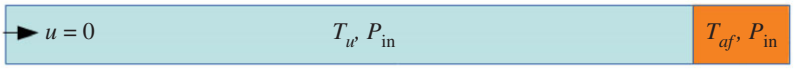

Figure 3. Set-up for the $D = 1$ burning velocity simulation. (Online version in colour.)

burning velocity is measured for various equivalence ratios ranging from $\phi = 0.5$ to $\phi = 2.25$. We use the laminar flame thickness δ_f at $\phi = 1$ for defining the reference length, where $\delta_f = (T_{af} - T_u)/\max(|dT/dx|)$. In order to accurately calculate the burning velocity, we use a long domain of $N \approx 90\delta_f$, which corresponds to 10^4 lattice points. In order to avoid the effect of the boundaries and transients due to initial acceleration, the flame speed S_L is measured when the flame front approaches the middle of the domain. The results are compared to the data provided by [27] from multiple experimental and computational sources in figure 4. It can be seen that flame speed computed by our model agrees well with the data available in the literature. Although there is considerable dispersion in the literature for the flame speed values for fuel-rich mixtures $\phi > 1$, the location of the peak burning velocity between $\phi = 1.5$ and $\phi = 2.0$ has been correctly captured. As is evident in figure 5, the profiles of temperature and mass fractions for $\phi = 0.5$ show a good match compared to the corresponding solution obtained from the 'FreeFlame' class of Cantera. This test case indicates that the present model is a promising candidate for simulating reactive flows with the lattice Boltzmann method.

(c) Circular expanding premixed flame

After confirming the one-dimensional behaviour of the model, we compute the two-dimensional circular expanding flame in a premixed hydrogen/air mixture with detailed chemistry. Similarly to the study [24,25], due to symmetry, only a quarter of the flame is solved. Symmetry boundary conditions are used on the left and bottom edges of the square domain while the characteristic based outlet boundary conditions [28,29] are imposed at the right and top edges of the domain. The bottom left corner is initialized with a burnt quarter sector at the adiabatic flame temperature $T_{af} = 1844.27$ K corresponding to the equivalence ratio $\phi = 0.6$. The rest of the domain is initialized with an unburnt mixture at the temperature $T_u = 298$ K. The composition in the burnt section is set to the equilibrium composition and the pressure in the entire domain is initialized to a uniform pressure $P = 5$ atm. For this premixed initial condition, the burning velocity is obtained as $S_L = 38.11\,\mathrm{cm\,s^{-1}}$ from solving a one-dimensional flame propagation set-up in Cantera. The flame thickness at these initial conditions is obtained as $\delta_f = 8.8 \times 10^{-3}$ cm. A square domain with the side $N \approx 51\delta_f$ was considered, which corresponds to 1200×1200 lattice points. The radius of the region initialized with the burnt equilibrium conditions is $R_{ig} \approx 8.5\delta_f$.

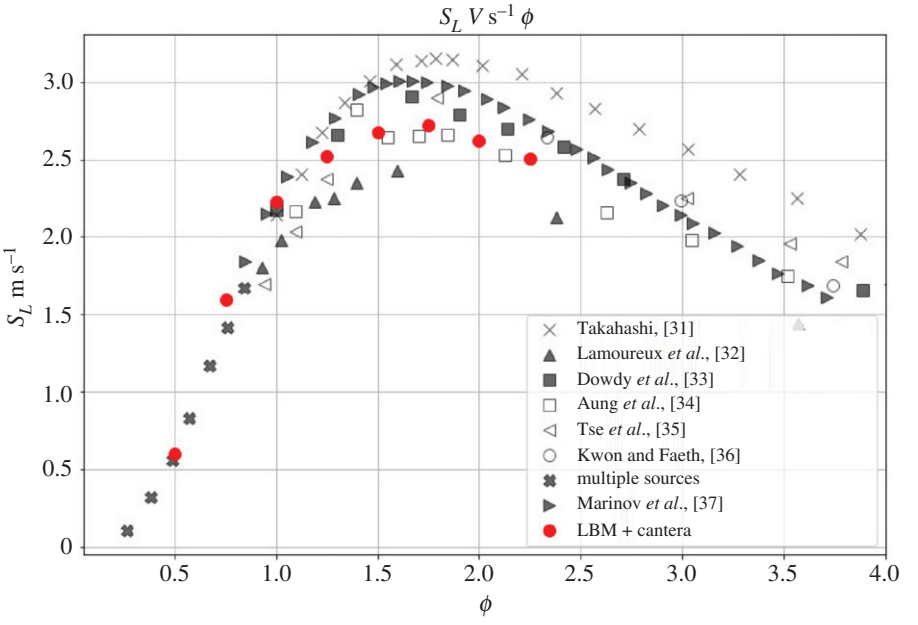

Figure 4. Burning velocity S_L versus equivalence ratio ϕ for the nine-species hydrogen/air mixture detailed chemistry [27]. (Online version in colour.)

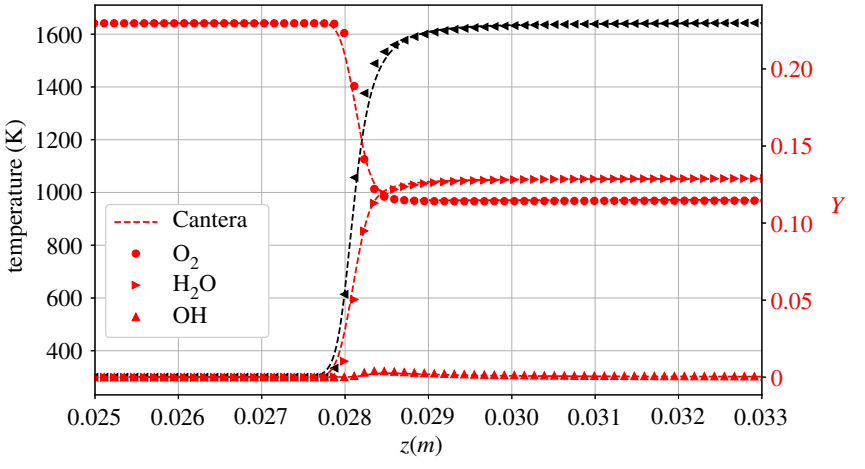

Figure 5. Profiles of temperature and mass fractions for one-dimensional planar flame at $\phi = 0.5$. (Online version in colour.)

The characteristic flame transit time is defined as $\tau = \delta_f / S_L = 2.31 \times 10^{-4}$ s [25]. Contours of temperature, velocity and mole fractions of oxygen and the hydroxide radical are shown at $t = 0.082\tau$ in figure 6*b*. As can be verified from figure 6*b*, the solution is not contaminated by numerical noise or anisotropies and the contours do not contain any other spurious features. The thin interface of the hydroxide radical at the flame front is captured correctly and the curvature of the flame is maintained. This is in contrast to e.g. [25], where the errors of the underlying numerical discretization leading to a spurious behaviour were reported when using Cartesian grids.

Next, we study the response of this set-up to a deterministic perturbation to validate the model with the Direct Numerical Simulation (DNS) of [25]. The initial circular profile of the flame is

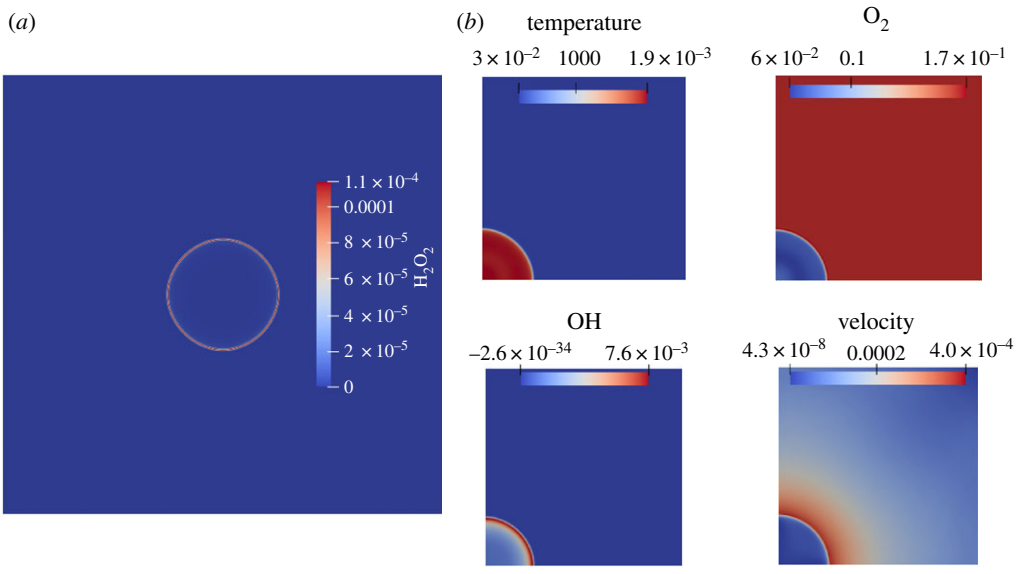

Figure 6. Premixed hydrogen/air circular outward expanding flame. (*a*) Contour plot of the mole fraction of H_2O_2 at $t = 0.082\tau$ obtained by reflecting about the left edge and the bottom edge of the domain, (*b*) Contours of temperature, mole fractions of O_2, OH and velocity at $t = 0.082\tau$. (Online version in colour.)

perturbed with a sinusoidal profile,

$$R(\theta) = R_{ig}(1 + A_0 \cos(4n_0\theta)), \tag{5.1}$$

where $n_0 = 4$ corresponds to the number of modes of the perturbation per $\pi/2$ sector of the flame and $A_0 = 0.05$ is the amplitude of the perturbation. The evolution of the perturbation is shown in figure 7. The heat release rate, $\dot{h}^c = -\sum_{a=1}^{M} H_a \dot{\rho}_a^c$, is a measure of the reactivity of the mixture. As it is evident in figure 7*a*, during the initial stages of the evolution, the perturbed modes are continuous and the heat release rate is uniform along the circumference of the flame. As explained in [25], the reactivity and therefore the heat release rate reduces at the crest due to diffusion and more consumption of the deficient reactant. This, along with the hydrodynamic instability due to the density ratio and the thermal-diffusive instability due to the heat and mass imbalance of the deficient reactant, leads to splitting of the peak of the crests into smaller cells, as is visible in figure 7*b*. A snapshot of the temperature contours over time shown in figure 7*c* verifies that the splitting of the flame indeed occurs from crests. Therefore, the splitting stems from the deterministic perturbation as expected, and not because of numerical noise. The mean radius of the flame is calculated by integrating along the flame front circumference,

$$\bar{R} = A^{-1} \int R \, \mathrm{d}A. \tag{5.2}$$

Here A is the circumferential length and R is the distance of the mean temperature isoline from the centre. On fitting $\bar{R} = at^{\alpha}$, the growth exponent was found to be $\alpha = 1.16$, in agreement with the results from DNS in the literature wherein the value of the exponent was found to be between almost linear [25] and 1.25 [30]. The local displacement speed [24,25] is calculated as

$$S_d = \frac{1}{\rho C_p |\nabla T|} \left[-\sum_{a=1}^{M} H_a \dot{\rho}_a^c + \nabla \cdot (\lambda \nabla T) - \rho \left(\sum_{a=1}^{M} C_{a,p} Y_a \delta \boldsymbol{u}_a \right) \cdot \nabla T \right]. \tag{5.3}$$

With the local flame normal $\boldsymbol{n} = -\nabla T/|\nabla T|$, the absolute propagation speed is calculated as $S_a = S_d + \boldsymbol{u} \cdot \boldsymbol{n}$. The density weighted displacement speed is defined as $\hat{S_d} = \rho S_d/\rho_u$, where ρ_u is the density of the unburnt mixture. The flame speeds are calculated as a mean over the flame

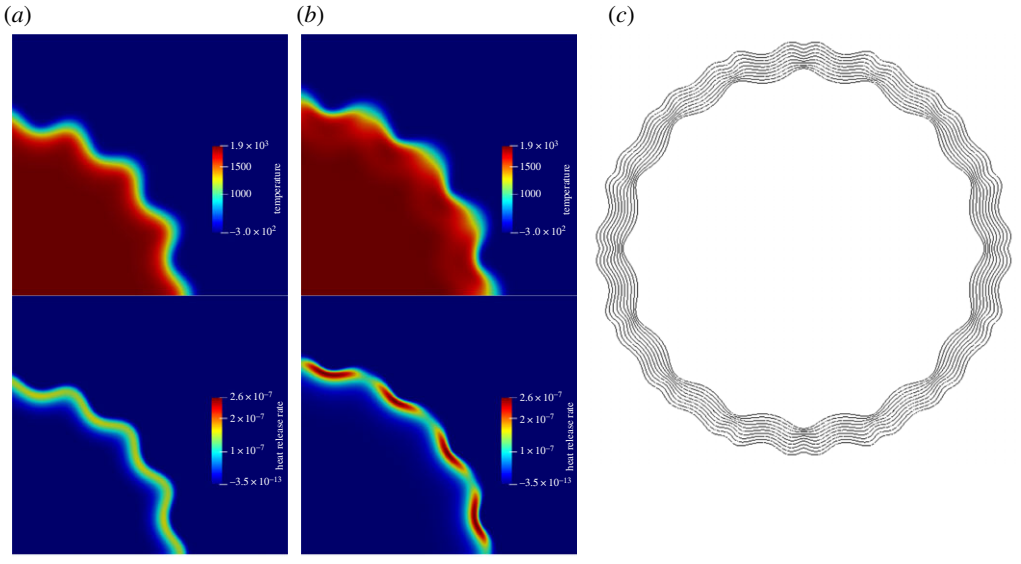

Figure 7. Contours of temperature and heat release rate. (*a*) $t = 0.024\tau$, (*b*) $t = 0.082\tau$, (*c*) line contours of $T = 1510.28$ K form $t = 0.041\tau$ to $t = 0.115\tau$. The domain has been reflected about the left and the bottom edge for plotting. (Online version in colour.)

interface isoline of $T = 3T_u$ in a way similar to equation (5.2). After the initial transients, the absolute propagation speed was found to reach a value of $6.2S_L$, whereas the density weighted displacement speed was found to fluctuate about $1.3S_L$. The corresponding values from the DNS results [25] are $7S_L$ and $1.5S_L$, respectively. The difference could be attributed to a number of factors including the type of grid, resolution, type of diffusion model, etc. Overall, the results agree well with the DNS [24,25].

6. Conclusion

In this paper, we proposed a lattice Boltzmann framework to simulate reactive mixtures. The novelty of the model lies in the fact that temperature and energy changes due to chemical reaction are handled naturally without the need of additional ad-hoc modelling of the heat of reaction. This was possible because of the thermodynamic consistency of the underlying multi-component model [11], which was extended to compressible reactive mixtures. The species interaction is modelled through the Stefan–Maxwell diffusion mechanism which has been extended in this work to accommodate the creation and destruction rates of the species due to chemical reaction. Computational efficiency has been achieved through reduced description of energy which makes it possible to describe the physical system by only $M + 2$ kinetic equations instead of $2M$ kinetic equations while retaining necessary physics such as the inter-diffusion energy flux. The model has been realized on the standard $D3Q27$ lattice, which not only reduces the computational costs compared to multispeed approaches but also possesses a wide temperature range, which is crucial for combustion applications.

The proposed model was validated in one and two dimensions with the 9-species 21 steps detailed hydrogen–air reaction mechanism. The accuracy of the model was assessed by calculating the burning velocity of a premixed hydrogen-air mixture in one dimension. The calculated flame speed agrees well with the results in the literature. The ability of the model to capture complex physics was tested by simulating a two-dimensional expanding circular flame. The circular flame simulation exhibited good isotropy and low numerical noise. The set-up was then subjected to monochromatic perturbations in order to study the evolution of the perturbed

flame. Good agreement with DNS simulations demonstrates viability of the proposed LBM for complex reactive flows.

Data accessibility. This article has no additional data.

Authors' contributions. N.S. implemented the model, ran the simulations and wrote the first draft of the manuscript. B.D. and I.V.K. supervised the project. All authors contributed to conceptualization of the model as well as writing, reading and approving the paper.

Competing interests. The authors declare that they have no competing interests.

Funding. This work was supported by the European Research Council grant no. 834763-PonD.

Acknowledgements. Computational resources at the Swiss National Super Computing Center CSCS were provided under grant no. s897. Authors thank Ch. Frouzakis at ETHZ for discussions about the circular expanding flame.

References

1. Krüger T, Kusumaatmaja H, Kuzmin A, Shardt O, Silva G, Viggen EM. 2017 *The lattice Boltzmann method*. Berlin, Germany: Springer International Publishing.
2. Succi S. 2018 *The lattice Boltzmann equation*. Oxford, UK: Oxford University Press.
3. Kang Q, Lichtner PC, Zhang D. 2006 Lattice Boltzmann pore-scale model for multicomponent reactive transport in porous media. *J. Geophys. Res.: Solid Earth* **111**, B05203.
4. Chiavazzo E, Karlin IV, Gorban AN, Boulouchos K. 2009 Combustion simulation via lattice Boltzmann and reduced chemical kinetics. *J. Stat. Mech.* **2009**, P06013.
5. Hosseini SA, Darabiha N, Thévenin D. 2018 Mass-conserving advection–diffusion lattice Boltzmann model for multi-species reacting flows. *Physica A* **499**, 40–57. (doi:10.1016/j.physa.2018.01.034)
6. Feng Y, Tayyab M, Boivin P. 2018 A Lattice-Boltzmann model for low-Mach reactive flows. *Combust. Flame* **196**, 249–254. (doi:10.1016/j.combustflame.2018.06.027)
7. Hosseini SA, Safari H, Darabiha N, Thévenin D, Krafczyk M. 2019 Hybrid lattice Boltzmann - finite difference model for low Mach number combustion simulation. *Combust. Flame* **209**, 394–404. (doi:10.1016/j.combustflame.2019.07.041)
8. Tayyab M, Zhao S, Feng Y, Boivin P. 2020 Hybrid regularized Lattice-Boltzmann modelling of premixed and non-premixed combustion processes. *Combust. Flame* **211**, 173–184. (doi:10.1016/j.combustflame.2019.09.029)
9. Hosseini SA, Abdelsamie A, Darabiha N, Thévenin D. 2020 Low-Mach hybrid lattice Boltzmann-finite difference solver for combustion in complex flows. *Phys. Fluids* **32**, 077105. (doi:10.1063/5.0015034)
10. Hosseini SA, Eshghinejadfard A, Darabiha N, Thévenin D. 2020 Weakly compressible lattice Boltzmann simulations of reacting flows with detailed thermo-chemical models. *Comput. Math. Appl.* **79**, 141–158. (doi:10.1016/j.camwa.2017.08.045)
11. Sawant N, Dorschner B, Karlin IV. 2021 Consistent lattice Boltzmann model for multicomponent mixtures. *J. Fluid Mech.* **909**, A1. (doi:10.1017/jfm.2020.853)
12. Karlin I, Asinari P. 2010 Factorization symmetry in the lattice Boltzmann method. *Physica A* **389**, 1530–1548. (doi:10.1016/j.physa.2009.12.032)
13. Saadat MH, Bösch F, Karlin IV. 2019 Lattice Boltzmann model for compressible flows on standard lattices: variable Prandtl number and adiabatic exponent. *Phys. Rev. E* **99**, 013306. (doi:10.1103/PhysRevE.99.013306)
14. Saadat MH, Karlin IV. 2020 Arbitrary Lagrangian–Eulerian formulation of lattice Boltzmann model for compressible flows on unstructured moving meshes. *Phys. Fluids* **32**, 046105. (doi:10.1063/5.0004024)
15. Saadat MH, Bösch F, Karlin I. 2020 Semi-Lagrangian lattice Boltzmann model for compressible flows on unstructured meshes. *Phys. Rev. E* **101**, 023311. (doi:10.1103/PhysRevE.101.023311)
16. Grad H. 1949 On the kinetic theory of rarefied gases. *Commun. Pure Appl. Math.* **2**, 331–407. (doi:10.1002/cpa.3160020403)
17. Thampi SP, Ansumali S, Adhikari R, Succi S. 2013 Isotropic discrete Laplacian operators from lattice hydrodynamics. *J. Comput. Phys.* **234**, 1–7. (doi:10.1016/j.jcp.2012.07.037)
18. Williams FA. 1985 *Combustion theory: the fundamental theory of chemically reacting flow systems*. Redwood City, CA: Benjamin/Cummings Pub. Co.

19. Goodwin DG, Speth RL, Moffat HK, Weber BW. 2018 Cantera: An Object-oriented Software Toolkit for Chemical Kinetics, Thermodynamics, and Transport Processes.
20. Kee RJ, Coltrin ME, Glarborg P. 2003 *Chemically reacting flow: theory and practice*. Hoboken, NJ: Wiley Pub. Co.
21. Wilke CR. 1950 A viscosity equation for gas mixtures. *J. Chem. Phys.* **18**, 517–519. (doi:10.1063/1.1747673)
22. Mathur S, Tondon PK, Saxena SC. 1967 Thermal conductivity of binary, ternary and quaternary mixtures of rare gases. *Mol. Phys.* **12**, 569–579. (doi:10.1080/00268976700100731)
23. Smith GP *et al.* 1999 GRI-Mech 3.0. See http://combustion.berkeley.edu/gri-mech/version30/text30.html.
24. Altantzis C, Frouzakis CE, Tomboulides AG, Boulouchos K. 2013 Numerical simulation of propagating circular and cylindrical lean premixed hydrogen/air flames. *Proc. Combust. Inst.* **34**, 1109–1115. (doi:10.1016/j.proci.2012.07.072)
25. Altantzis C, Frouzakis CE, Tomboulides AG, Boulouchos K. 2015 Direct numerical simulation of circular expanding premixed flames in a lean quiescent hydrogen-air mixture: phenomenology and detailed flame front analysis. *Combust. Flame* **162**, 331–344. (doi:10.1016/j.combustflame.2014.08.005)
26. Li J, Zhao Z, Kazakov A, Dryer FL. 2004 An updated comprehensive kinetic model of hydrogen combustion. *Int. J. Chem. Kinet.* **36**, 566–575. (doi:10.1002/kin.20026)
27. Dahoe AE. 2005 Laminar burning velocities of hydrogen–air mixtures from closed vessel gas explosions. *J. Loss Prev. Process Ind.* **18**, 152–166. (doi:10.1016/j.jlp.2005.03.007)
28. Poinsot TJ, Lelef SK. 1992 Boundary conditions for direct simulations of compressible viscous flows. *J. Comput. Phys.* **101**, 104–129. (doi:10.1016/0021-9991(92)90046-2)
29. Feuchter C, Wagner O, Stief A, Beisswenger T. 2019 Turbulent flow simulations around a surface-mounted finite cylinder using an entropic multi-relaxation lattice Boltzmann method. *Fluid Dyn. Res.* **51**, 055509. (doi:10.1088/1873-7005/ab3baf)
30. Liberman MA, Ivanov MF, Peil OE, Valiev DM, Eriksson LE. 2004 Self-acceleration and fractal structure of outward freely propagating flames. *Phys. Fluids* **16**, 2476–2482. (doi:10.1063/1.1729852)
31. Takahashi F, Mizomoto M, Ikai S. 1983. Alternative energy sources III. In *Nuclear energy/synthetic fuels*, vol. 5 (ed. T Nejat Veziroglu), pp. 447–457. New York, NY: McGraw-Hill.
32. Lamoureux N, Djebaili-Chaumeix N, Paillard CE. 2002. Laminar flame velocity determination for H_2–air–steam mixtures using the spherical bomb method. *Journal de Physique de France IV* **12**, 445–452.
33. Dowdy DR, Smith DB, Taylor SC, Williams A. 1990. The use of expanding spherical flames to determine burning velocities and stretch effects in hydrogen–air mixtures. In *Twenty-third symposium (international) on combustion, Orléans France, 22–27 July 1990*, pp. 325–332. Pittsburgh, PA: The Combustion Institute.
34. Aung KT, Hassan MI, Faeth GM. 1997. Flame stretch interactions of laminar premixed hydrogen/air flames at normal temperature and pressure. *Combustion and Flame* **109**, 1–24.
35. Tse SD, Zhu DL, Law CK. 2000. Morphology and burning rates of expanding spherical flames in H_2/O_2/inert mixtures up to 60 atmospheres. *Proceedings of the Combustion Institute* **28**, 1793–1800. (doi:10.1016/S0082-0784(00)80581-0)
36. Kwon OC, Faeth GM. 2001. Flame/stretch interactions of premixed hydrogen-fueled flames: measurements and predictions. *Combustion and Flame* **124**, 590–610.
37. Marinov NM, Westbrook CK, Pitz WJ. 1996. Detailed and global chemical kinetics model for hydrogen. In *Transport phenomena in combustion*, vol. 1 (ed. S Chan), pp. 118–129. Washington, DC: Taylor & Francis.